



UNIVERSITY OF LEEDS

This is a repository copy of *Development of DLC coating architectures for demanding functional surface applications through nano- and micro-mechanical testing*.

White Rose Research Online URL for this paper:
<https://eprints.whiterose.ac.uk/87850/>

Version: Accepted Version

Article:

Beake, BD, Liskiewicz, TW orcid.org/0000-0002-0866-814X, Vishnyakov, VM et al. (1 more author) (2015) Development of DLC coating architectures for demanding functional surface applications through nano- and micro-mechanical testing. *Surface and Coatings Technology*, 284. pp. 334-343. ISSN 0257-8972

<https://doi.org/10.1016/j.surfcoat.2015.05.050>

© 2015, Elsevier. Licensed under the Creative Commons Attribution-NonCommercial-NoDerivatives 4.0 International <http://creativecommons.org/licenses/by-nc-nd/4.0/>

Reuse

Items deposited in White Rose Research Online are protected by copyright, with all rights reserved unless indicated otherwise. They may be downloaded and/or printed for private study, or other acts as permitted by national copyright laws. The publisher or other rights holders may allow further reproduction and re-use of the full text version. This is indicated by the licence information on the White Rose Research Online record for the item.

Takedown

If you consider content in White Rose Research Online to be in breach of UK law, please notify us by emailing eprints@whiterose.ac.uk including the URL of the record and the reason for the withdrawal request.



eprints@whiterose.ac.uk
<https://eprints.whiterose.ac.uk/>

Development of DLC coating architectures for demanding functional surface applications through nano- and micro-mechanical testing

B.D. Beake^{1,*}, T.W. Liskiewicz², V.M. Vishnyakov³ and M.I. Davies¹

¹ Micro Materials Ltd., Willow House, Yale Business Village, Ellice Way, Wrexham, LL13
7YL, UK

² Institute of Functional Surfaces, School of Mechanical Engineering, University of Leeds,
Woodhouse Lane, Leeds, LS2 9JT, UK

³ School of Computing and Engineering, University of Huddersfield, Queensgate,
Huddersfield, HD1 3DH, UK

* Corresponding author. Email: ben@micromaterials.co.uk. Tel: +44 1978 261615.

Abstract

DLC coatings can combine high hardness with low friction. However, they are often deposited with high levels of intrinsic stress and display low adhesion strength resulting in poor performance in demanding applications. A highly topical challenge is to develop advanced DLC coatings capable of withstanding more demanding applications in the automotive, cutting tools, MEMS and oil and gas sectors. The results from several nanomechanical and tribological test techniques - nanoindentation, nano-scratch and nano-fretting (nano-wear) - can be used together to aid the design of DLC coating architectures for enhanced durability in specific applications. In this study the behaviour of multilayered DLC coatings (Cr/W-C:H/a-C:H, Cr/W-C:H/Si-a-C:H) was compared to that of CrN/a-C:H:W (WC/C). We have previously reported that in nano-wear tests the coating with the highest hardness and H/E displayed greater wear resistance [T.W. Liskiewicz et al, *Surf. Coat. Technol.* 237 (2013) 212]. By employing nano- and micro-scale tribological testing with probes of differing sharpness it is possible to change the sensitivity of the test to probe the response of the coating top layer or the entire multilayer coating-substrate system. In the nano-scratch tests using a spherical indenter with a 5 μm end radius the maximum stresses are located well within the top layer of the multilayer coatings and consequently the mechanical properties of this top layer dominate the nano-tribological behaviour. In the micro-scratch using a 25 μm spherical probe the stress field extends further towards the sub-layers and steel substrate and consequently the behaviour is completely different. Under these conditions the coating with the lowest hardness and H/E showed improved performance with higher critical loads for cracking and total coating failure. High resolution SEM imaging has been used to investigate this further. A simple contact model strongly suggests that cracking and failure events occur on the harder coatings when the maximum von Mises stress was located close to the interfaces in the multilayer systems.

1. Introduction

Diamond-like carbon (DLC) is a metastable form of amorphous carbon and has a mixture of sp^3 and sp^2 bonding and the mechanical properties of DLC films vary with sp^2/sp^3 ratio [1]. A wide range of available amorphous carbon coating architectures and a number of possible deposition methods allow tailoring of the coating functionality to many demanding functional surface applications. DLC coating properties include high hardness, low friction, electrical insulation, anti-corrosion, chemical inertness, optical transparency, biological compatibility, ability to absorb photons selectively, smoothness and resistance to wear. Hence, DLC coatings have found many practical applications across industrial sectors, including razor blades, computer hard drives, silicon solar cells, MEMS applications, orthopaedic implants, optical lenses, and finally cutting tools and internal combustion engine components [2].

Improved resolution and efficiency of DLC coating testing techniques is needed for development of new demanding applications and accurate nano-mechanical characterisation is a critical step in DLC coating efficient optimisation. Analytical tools for nano-scale materials testing have rapidly developed over the last decades and integration of measurement data obtained from nano-mechanical testing provides reliable inputs to improved predictive coating wear models [3,4].

In order to tailor DLC coatings for demanding functional surface applications it is necessary to optimise the coating tribological behaviour, which has been extensively studied in the literature. Gies et al. deposited homogeneous and gradient a-C:H:W coatings on steel and determined their mechanical properties using nanoindentation and reciprocating wear test with nanometre resolution [5]. The authors showed better performance in micro- and macro-wear tests of the gradient coating systems and proposed an improved wear model taking into account the changing stress fields during the wear tests. Almost two decades ago, Jiang and

Arnell looked at running-in behaviour of DLC coatings using ball-on-disk apparatus [6]. A classical running-in wear curve with a transition in wear rate from a high initial rate to a low rate with sliding was observed. It was also found that variations in friction coefficient with sliding distance were not related with this transition in wear rate and a transfer film was rapidly developed on the uncoated ball surface. Gåhlin et al. reviewed and discussed ME-C:H coatings applications in motor vehicles [7]. They found out that over time, Me-C:H coatings contributed to significant decrease of friction and dramatic increase of wear resistance and resistance to seizure in these applications. More recently, Zeng et al. compared three types of high wear resistant carbon composite coatings by exploring the influence of a sputter-chemical vapour deposition hybrid process on coating properties [8]. The authors showed that it possible to optimise the deposition process by using pure Argon atmosphere resulting in coating with exceptionally high load-bearing capacity and excellent wear resistance attributed to its excellent adhesion, high toughness and low friction coefficient.

The authors of this paper have also performed a more complete characterisation of carbon coatings by combining the results of the nanoindentation tests with additional nano-mechanical and nano-tribological test capability, namely nano-scratch, nano-impact and nano-wear [9-11]. These tests provided complementary information about the durability of DLC films in these more complex mechanical loading situations. It was shown that substrate yield can play a key role in the nano-tribological behaviour, particularly for ultra-thin films on Silicon. By performing repetitive nano-scratch tests at a sub-critical load it was possible to tune the maximum stress close to the coating-substrate interface so that the test was more sensitive to high stress in the film and at the interface.

In this paper the behaviour of three multi-layered DLC coatings is studied by nanoindentation, nano-scratch and micro-scratch testing. The multilayered coatings were Cr/W-C:H/a-C:H, Cr/W-C:H/Si-a-C:H and CrN/a-C:H:W (WC/C). In the Cr/W-C:H/a-C:H

and Cr/W-C:H/Si-a-C:H coating systems the adhesion layer is a thin Cr and then gradient layers are applied to adapt the E-modulus of the soft substrate to the E-modulus of the hard top coating, thus giving the coating both abrasive wear resistance and impact fatigue wear resistance (flexibility/toughness). In the WC/C system the hard CrN sublayer provides load support and improved adhesion. Nanomechanical characterisation provides detailed mechanical property data including the elastic modulus and plasticity of the coating systems in addition to hardness determination. The nanomechanical properties of DLC films commonly show a strong correlation with the wear resistance of the DLC films in dry sliding or impact conditions. Nanotribological characterisation by nano- and micro-scratch testing with the modelling approach described provides direct access to the contact pressure so that peak stresses can be determined. The ratio of the hardness to modulus (H/E) has been found to correlate with tribological behaviour more closely than hardness alone with several reports of higher H/E being generally beneficial in sliding/abrasion [12-14]. In this work the relationship between the plasticity index (PI) and the ratio of hardness to reduced modulus (H/E_r) has been investigated for the different coatings. The correlation with H/E_r rather than H/E is explored in this publication since it is E_r rather than E that is directly determined from the unloading curve analysis using non-rigid indenters. By employing nano- and micro-scale tribological testing with probes of differing sharpness it is possible to change the sensitivity of the test to probe the response of the coating top layer or the entire multilayer coating-substrate system. High resolution SEM imaging has been used to provide further details on the deformation mechanisms and a simple contact model correlating the position of the maximum in the von Mises stress with the coating-substrate interface is explored. In the nano-scratch tests using a spherical indenter with a 5 μm end radius the maximum stresses are located well within the top layer of the multilayer coatings and consequently the mechanical properties of this top layer dominate the nano-tribological behaviour. In the

micro-scratch using a spherical indenter with a 25 μm end radius the stress field extends further towards the sub-layers and steel substrate. With increasing load the maximum stress can be positioned at different interfaces in the multilayer system to investigate any potential deficiencies in adhesion between different layers.

2. Experimental

2.1 Materials

A series of three DLC coatings with varied mechanical properties was deposited on M2 grade steel substrates for this study. Multilayer coatings with a-C:H and Si-a-C:H top layers were deposited using the industrial scale PECVD Flexicoat 850 system (Hauzer Techno Coating, the Netherlands) in the Advanced Coatings Design Laboratory in School of Mechanical Engineering at the University of Leeds while a multilayer WC/C was a commercial coating, Balinit C Star, obtained from Oerliken Balzers company. The a-C:H and Si-a-C:H coatings deposited with chromium and graded tungsten carbide interlayers in order to enhance adhesion between the DLC coating and the substrate. The Cr layer was deposited using magnetron sputtering, while the WC layer was deposited using magnetron sputtering with the gradual introduction of Acetylene gas to the complete PACVD stage, thus creating a functional gradient layer in one continuous deposition process. Additionally, Si-a-C:H was doped with silicon using hexamethyldisiloxane (HMDSO) precursor. According to Oerliken Balzers specification, Balinit C Star is applied in a single-pass vacuum process at temperatures between 180 and 350 $^{\circ}\text{C}$, resulting in homogeneous coating structure. Thickness of the coatings was assessed using Calotester (Tribotechnic, France) employing abrasion ball cratering testing method. Full details of the coating architecture are given in Table 1 below, and are referred to in this publication by their top layer composition for convenience.

[Table 1 about here]

2.2 Nanoindentation, nano-scratch and micro-scratch testing

Nanoindentation, nano-scratch and micro-scratch testing were performed using the NanoTest Vantage (from Micro Materials Ltd., Wrexham, UK). Nanoindentation experiments were performed in order to characterise the hardness and Young's modulus of the coatings. ISO 14577-4 recommends that measurements should be made across a range of indentation loads to enable film-only values of hardness and elastic modulus to be determined. In particular, it cautions that measurements at an indentation depth of 10 % of the film thickness provide a good estimate of the coating hardness but will contain some contribution from the elastic properties of the underlying substrate. The experiments were performed on the three coatings with a sharp Berkovich indenter to peak loads of 1, 3, 5, 10, 20, 30, 40, 50...100 mN with 10 repeats for each load. The loading time was 20 s with a hold of 5 s at peak load before unloading in 20 s. Data were corrected for thermal drift using hold periods of 60 s prior to the load ramp and after 90 % unloading. The area function of the indenter and frame compliance were calibrated using fused silica and single crystal tungsten reference samples. Hardness, reduced modulus, elastic work (W_e) and plastic work (W_p) were measured over the contact depth range corresponding to 1-100 mN so that the relationship between the plasticity index (PI), the H/E_r and the apparent constant of proportionality in Equation 1 when using a Berkovich indenter could be determined.

$$PI = W_p / (W_p + W_e) = 1 - x(H/E_r) \quad [\text{Eqn. 1}]$$

where x is a constant and E_r is the reduced indentation modulus.

Progressive load (3-scan, topography-scratch-topography) nano-scratch tests to 500 mN were performed using a spheroconical diamond probe of end radius 5 μm . The probe radius was

calibrated by spherical indentation testing on fused silica. The nano-scratch procedure involved 3 sequential scans, topography-scratch-topography, at 2.5 $\mu\text{m/s}$, always in the same direction. These were (i) pre-scan: scanning at 0.1 mN over a 500 μm track (ii) progressive load scratch: the load is low (0.1 mN) over the first 50 μm scan then ramping at a constant rate of 2.9 mN/s to reach 500 mN just before the end of the scan (iii) post-scan, with the same low load as the pre-scan. 5 scratch tests were done on each coating with adjacent tracks separated by 100 μm . By performing three-scan progressive load nano-scratch tests it is possible to determine the critical load for the onset of non-elastic deformation since this is the load at which the residual scratch depth is no longer zero.

Micro-scratch testing to 5 N was performed using a similar 3-scan procedure using a spheroconical diamond probe of end radius 25 μm . The probe radius was calibrated by spherical indentation testing on fused silica. The procedure involved 3 sequential scans, topography-scratch-topography, at 20 $\mu\text{m/s}$, always in the same direction. These were (i) pre-scan: scanning at 10 mN over a 1000 μm track (no wear occurs at this load with a 25 μm probe) (ii) progressive load scratch: the load is low (10 mN) over the first 50 μm scan then ramping at a constant rate of 107 mN/s to reach 5 N just before the end of the scan (iii) post-scan, with the same low load as the pre-scan. 5 scratch tests were done on each sample, with adjacent tracks separated by 100 μm . Sample roughness was determined over a 330 μm scan length taken from the pre-scans. The R_a surface roughness was found to be 10.9, 11.3 and 11.5 nm for the a-C:H, Si-a-C:H and a-C:H:W coatings respectively (mean values are averages of five repeats). Friction was also measured during the nano- and micro-scratch tests using calibrated tangential force sensors. A Zeiss Supra40VP Field Emission Gun SEM system was used for high-resolution microscopic analysis of the nano- and micro-scratch tracks.

The probe depth data (either on-load or residual) are shown (in figure 4(b-c)) after removal of any slope, topographic and the instrument compliance contribution to the measured deformation, i.e. true depth data. The mean pressure during the nano- and micro-scratch tests was estimated by the application of a Hertzian treatment previously applied to the nano-scratch testing of carbon films with spherical probes [15,16]. The method enables the yield stresses and the pressure required for the failure of the film to be estimated from contact mechanics, assuming the geometry of indentation, provided spherical indenters are used. The contact depth (h_c) in a spherical indentation contact is given by

$$h_c = (h_t + h_r)/2 \quad [\text{Eqn. 2}]$$

where h_c is the contact depth, h_t is the on-load scratch depth and h_r is the residual depth from the final scan. The contact radius (a) is determined from Equation 3, where R is the indenter radius.

$$a = \sqrt{(2Rh_c - h_c^2)} \quad [\text{Eqn. 3}]$$

$$P_m = L/\pi a^2 \quad [\text{Eqn. 4}]$$

The contact pressure, P_m , at any point along the scratch track is given by equation 4, where L is the applied load. To apply this approach to the nano-scratch data it is necessary to assume that: (i) the presence of a tangential load does not influence the pressure distribution too greatly so that the measured friction coefficient is well below 0.3 (ii) the radius of the indenter is constant (iii) the sliding speed is sufficiently slow and contact sufficiently close to elastic that the load is supported on the rear of the indenter (iv) the indenter can reach the

bottom of the scratch track in the final topographic scan. It is also important that the test instrumentation has sufficiently high lateral rigidity (as the NanoTest Vantage) so that when using a sensitive friction transducer the scratch track is not significantly affected by surface roughness. The method has previously been validated for DLC films deposited on Silicon with good agreement found between scratch track widths determined from the analytical method and assessed by microscopic examination [16].

3. Results

3.1 Nanoindentation

Nanoindentation revealed clear differences in mechanical behaviour between the different DLC coatings. As an illustration the results from tests to 40 mN peak load are shown in Table 2. The a-C:H coating had the highest hardness, modulus, H/E_r , H^3/E_r^2 and lowest plasticity index. Measurements of hardness and reduced modulus vs. depth [previously reported in ref. 3] show that the hardness of the three coatings decreases at very low indentation depths, reflecting non-fully developed plasticity in the contact (i.e. the mean pressure developed in the contact is less than the actual hardness of the film, as described in detail in ISO14577-4). The measured reduced elastic modulus increases with increasing indentation depth for Si-a-C:H and a-C:H:W but slightly decreases for a-C:H. The depth-dependence of the relationship between plasticity index (PI), H/E_r and the apparent constant of proportionality when using a Berkovich indenter is shown in Figure 1(a-c). The relationship between PI and H/E_r for the coatings at a contact depth of 300 nm is shown in Figure 1(d). There is a linear relationship over this range of H/E_r with $R^2 = 1$.

[Fig. 1 and Table 2 about here]

3.2 Nano-scratch tests with $R = 5 \mu\text{m}$ probe

The critical load (L_y) was determined from the depth data as the load where the residual corrected depth is non-zero.

[Fig. 2 and Table 3 about here]

The load-dependence of friction coefficient in nano-scratch test using $R = 5 \mu\text{m}$ probe is shown in Figure 2. The friction coefficient at yield is shown in Table 3. SEM images are shown in Figure 3. The a-C:H and Si-a-C:H show semi-circular cracks at the rear of the contact extending across the entire scratch track. For coatings A and B the onset of cracking at L_{c1} was accompanied by an inflexion in the residual depth data. The inflexion in depth was more pronounced on the a-C:H coating. L_{c1} values were (422 ± 4) mN and (445 ± 12) mN for a-C:H and Si-a-C:H respectively. a-C:H:W did not show L_{c1} failure before 500 mN. The L_{c2} failure (total failure of the coating) was not reached before 500 mN on any of the coatings.

3.3 Micro-scratch tests with $R = 25 \mu\text{m}$ probe

Figure 4 (a) shows (a) the L_{c1} and L_{c2} critical loads for each of the three coatings. The ranking is the same for both critical loads, with the highest values on a-C:H:W and the lowest on Si-a-C:H. Fig. 4 (b)-(e) show illustrative behaviour from a test on each of the coatings. Fig. 4 (b) shows the on-load probe depth, (c) residual depth, (d) the corresponding load-dependence of elastic recovery. Fig 4.(e) shows the variation in friction coefficient with applied load. Prior to L_{c1} failure the on-load and residual depth data are very similar for all three coatings (fig. 4(b-c)). The dependence of the friction at L_y , L_{c1} and L_{c2} is summarised in Fig. 4 (f). The frictional response of a-C:H and Si-a-C:H is very similar frictional behaviour, with friction coefficients of (0.075 ± 0.002) and (0.073 ± 0.003) respectively at yield. The a-C:H:W has

higher friction of (0.100 ± 0.006) at yield. The friction coefficient gradually increases with applied load following the same trend for all the coatings (figure 4 (e)), with the data on a-C:H:W being about 0.03 higher.

Figure 5 shows SEM images of micro-scratch tracks. A complex deformation with cracks in front, behind and at the side of the contact zone is observed on a-C:H (fig. 5(a)). The crack pattern on a-C:H:W is very different to that on the other two coatings. A network of fine cracks is produced that appears to follow the microstructure. Although there is spallation and chipping outside the scratch track it appears reduced in comparison to that observed on the a-C:H and Si-a-C:H coatings.

[Table 4 about here]

4. Discussion

4.1 Nanoindentation and plasticity

There was a marked correlation between the nanomechanical behaviour of the coatings and their tribological response in nano- and micro-scale scratch testing. Nanoindentation data at different peak loads contain differing elastic contribution from the M2 substrate (and sub-layers). The measured reduced elastic modulus increases with increasing indentation depth for Si-a-C:H and a-C:H:W but slightly decreases for a-C:H. This is due to the influence of the steel substrate which is stiffer than Si-a-C:H or a-C:H:W but slightly lower modulus than a-C:H. To obtain accurate values of the elastic modulus of the top layer, it is necessary to remove this substrate component which exists even when indenting to 1/10 of the coating thickness. Measurements at a range of indentation depths are extrapolated to zero depth to provide a measure of the coating-only modulus following the procedure in ISO14577. The

reduced indentation moduli for the top-layer were 202, 140 and 130 GPa (which correspond to Young's moduli of 235, 153 and 140 GPa respectively assuming the Poisson's ratio of the film is 0.2). The relationship between plasticity index and H/E_r (Equation 1) was investigated over a wide load range (fig. 1 (a-c)). Although similar relationships could be determined for H/E instead of H/E_r we have chosen to report H/E_r since this is the primary output from the nanoindentation curve and so does not require exact knowledge of the coatings' Poisson's ratios. On these coatings H/E_r varied little with load over this depth range so changes in plasticity and proportionality constant primarily reflect the effect of changing indenter geometry over this depth range. There appear to be two regimes with x being constant above about 250 nm and increases as the depth is reduced below this. For loads and penetration depths where the indenter is self-similar the relationship between H/E_r and plasticity is robust and the apparent constant varies very little across a wide load range. However, at smaller depths the rounding of the Berkovich indenter influences this relationship and lower plasticity and higher values of x are found. Figure 1(d) shows the relationship at a contact depth of 300 nm where x is constant vs. depth so the rounding of the Berkovich is not significant. The type of DLC influences the value of the proportionality constant. The a-C:H coating has a plasticity index of 0.30 and $x \sim 5.4$, Si-a-C:H has plasticity index of 0.36 and $x \sim 5.7$ and a-C:H:W has a plasticity index of 0.48 and $x \sim 6.5$. Since it relates the H/E_r in the contact to the plasticity index the proportionality constant contains a contribution from the substrate ($x \sim 6.6$ for hardened steel). At low relative indentation depth the substrate contribution is minimal and the observed differences in x are due to differences in coating properties. FE analysis has predicted $x \sim 5$ [17-18] whilst for bulk materials experimental evidence suggests that $x \sim 5$ for glasses and $x \sim 6-7$ for metals [19-20]. For hard coating systems x has been reported to be ~ 6.4 on TiN-based nanocomposites [21] and 5.7 on TiAlCrN/TiAlCrSiYN multilayers [22]. Based on theoretical and experimental studies it has been suggested that PI , h_r/h_m and H/E

essentially contain the same information and can be used interchangeably [19-20]. However, although they are well correlated there appear to be some subtle differences. The three coatings studied here show slightly lower PI than h_r/h_m with the difference being greatest for a-C:H, i.e. the coating with highest H/E (max. difference = 0.05). The reasons for the different values of x between the coatings are that the equation is not exact and deviations become more apparent at higher H/E . There may also be some influence from surface roughness, pile-up/sink-in or the fact that the energy based equations use the energy to the maximum depth whilst hardness from unloading curve analysis is determined at the contact depth [23].

Although much softer than nitride coatings such as TiAlN, the a-C:H:W coating has similar plasticity and x . It can be considered as metal-doped and in terms of plasticity it has the character of more ceramic coating which may well be connected to its high load carrying capacity without cracking in highly loaded contact. DLC coatings typified by the a-C:H coating are hard and elastic, having high H , H/E and Y/E . Tabor determined a constraint factor C , connecting hardness and yield stress according to $H = CY$ [24]. Based on experiments on metals a value of 2.8 was found to be a good fit experimentally. However, for higher Y/E materials such as the coatings tested here much lower values are found.

The Si-a-C:H and especially a-C:H:W coatings have lower hardness and higher plasticity, a combination which has been associated with improved crack resistance in scratch testing in amorphous hydrogen-free carbon coatings [25-28]. Although the a-C:H:W coating is softer it has a higher threshold for cracking when tested with $R = 5$ and $25 \mu\text{m}$ probes. Plastic flow can be considered as the major source of stress relaxation in the coating system. Although plasticity is not the same as toughness, as discussed in detail elsewhere [19, 21, 26-28], nevertheless in practice it appears that the two properties are well correlated. Where high

fracture toughness is associated with high H^3/E^2 then this appears to be a consequence of the higher load-support (the critical load for plastic flow is connected to H^3/E^2) so that for a given load the total deformation is lower so the bending stresses in the coating are reduced rather than intrinsic structural toughening.

4.2 Nano-scratch behaviour ($R = 5 \mu\text{m}$)

Based on Johnson's contact mechanics analysis the critical load should scale with H^3/E^2 on bulk materials [12, 30]. For these coatings there was a strong but non-linear dependence on H^3/E^2 and H/E (Tables 2 and 3). The coating yield stress has been estimated from the nano-scratch test data. The Hertzian analysis is well suited to the nano-scratch testing of DLC films with spherical probes with an end radius of $5 \mu\text{m}$ or greater due to their intrinsic low friction and high H/E so that contact remains elastic or close to it over a wide load range. Plastic deformation in the sample beneath a spherical indenter can be first expected to occur when $P_m \sim 1.1Y$ at a depth of $\sim 0.47a$ [24, 29, 30]. The mean pressure at yield (P_m) has been converted to a yield stress, Y , using the relationship that $Y = P_m/1.1$. Table 5 shows a comparison between the yield stress determined from the nano-scratch tests with the 5 micron probe and the yield stress determined from an analytical analysis of the nanoindentation test data with the Berkovich indenter. Although the indenter geometry in the two types of tests is different, in both cases the yield occurs well within the coating. The simplifying assumptions that (i) the test probe radius is constant vs. depth (ii) that friction was sufficiently low that the stress field is not too different from that in a spherical indentation (iii) the lateral rigidity of the instrumentation is high enough, are well met. There is reasonably good agreement, especially for Si-a-C:H and a-C:H:W.

[Table 5 about here]

Although at yield the depth under load is highest on the a-C:H (Table 3), as the yield occurs at markedly different critical loads on the three coatings this reflects the much higher critical load for this coating (206 mN). When comparing the depth at a given applied load then the trend is reversed and a-C:H shows the smallest on-load and residual depths.

4.3 Micro-scratch behaviour ($R = 25 \mu\text{m}$)

By employing a larger radius test probe it is possible to change the sensitivity of the test to probe the response of the entire multilayer coating-substrate system. The feasibility of this has been investigated by Schwarzer and co-workers for scratch testing thicker monolayer and multilayer coating systems on cemented carbide where the total thickness of the coating layers was 10-11 μm with test probe radii the range 20-200 μm [31]. For the instrumentation used in that study it was reported that the combination of high surface roughness of the coatings and insufficient resolution made it impossible to detect the onset of plastic flow. In contrast, in this current study the DLC coatings were smoother and the test instrumentation is optimised for nano-/micro-scale testing having high sensitivity and lateral rigidity so that it is trivial to determine reliably the critical load for plastic flow from the point at which the residual depth is no longer zero. On other coating systems and bulk materials (e.g. thin carbon coatings on Si, Si [9-11]) we have found no evidence that any significant yield occurs below this and have reported good agreement between the mean pressures determined at yield both with literature and the results of nanoindentation tests.

In contrast to the behaviour with the $R = 5 \mu\text{m}$ probe the yield and failure pressures with the $R = 25 \mu\text{m}$ probe are increasingly dominated by substrate deformation. The maximum von Mises stress at L_y is located at a depth well within the top coating layer. However, it is likely that failure occurs on exceeding the substrate yield stress. The critical load for yield is not

higher for the a-C:H coating despite its much higher hardness since the significant part of the deformation is due to elastic deformation of the substrate. The a-C:H:W coating showed higher load support without cracking. The higher L_{c1} and L_{c2} do not equate to significantly greater mean pressure in the contact, but due to the higher load the stress field was able to develop deeper into the substrate before the onset of cracking.

In a tribological system toughness may be at least as important as hardness. An interesting concept for providing a qualitative assessment of differences in coating toughness has been proposed by Zhang and co-workers [28, 32, 33]. They equated L_{c1} with the resistance to the initiation of cracks and $(L_{c2}-L_{c1})$ as a measure of the toughness (L_{c2} = load for total failure). They defined a parameter representing resistance to crack initiation and also propagation as follows (Eqn. 5):-

$$\text{scratch crack propagation resistance parameter (CPR)} = L_{c1}(L_{c2}-L_{c1}) \quad [5]$$

Although absolute values of this parameter, later called “scratch toughness” [28], are highly dependent on the radius of the test probe nevertheless it can provide a useful qualitative assessment of coating response. The CPR values were (1.0 ± 0.4) , (0.8 ± 0.2) and (2.3 ± 0.7) N^2 for the a-C:H, Si-a-C:H and a-C:H:W coatings respectively. Higher L_{c1} and L_{c2} correspond to a tougher coating despite having lower H^3/E^2 . There is a correlation between H^3/E^2 and failure with lower H^3/E^2 coatings being able to deform more elastically prior to the L_{c2} failure. Zhang and co-workers have studied several metal-doped nc-Me_nN/a-SiN_x coating systems where improved scratch toughness was found to be at the expense of hardness [26-28]. In nano-scratch testing it is commonly observed for a hard coating deposited on a hard and brittle substrate that higher hardness, H/E and H^3/E^2 is correlated with lower scratch depths at low load but a lower L_{c2} . Reported examples of coating systems showing this behaviour include 1 μm a-C on Si in nano-scratch testing with a $R = 4 \mu\text{m}$ probe [25] and

~0.8 μm nc-TiN/a-SiN_x on Si in nano-scratch testing with a $R = 3 \mu\text{m}$ probe [34]. When micro-scratch testing of hard nitride coatings on cemented carbide the on-load scratch depths do not vary significantly with coating properties but the same trend of higher hardness, H/E and H^3/E^2 being connected with a lower L_{c2} is also commonly found [21, 35-37].

[Table 6 about here]

4.4 Deformation mechanism in the scratch test

To further understand the interrelationships between plasticity, load support, scratch recovery and cracking a simple contact model has been applied to estimate the magnitude and location of the maximum von Mises stress at the different critical loads for each of the coatings in the micro-scratch test. The mean pressure vs. applied load determined by the Hertzian analysis of micro-scratch test data is shown in Figure 6 (a). The mean pressure at yield is around 14-16 GPa. As the applied load increases the decrease in pressure towards ~12 GPa is due to a greater contribution from the softer layers and substrate together with added complexity from cracking/yield.

The analysis suggests that at the L_{c2} failure the maximum von Mises stress is located below the free surface at a depth of around 3.9, 3.7 and 4.8 μm for the a-C:H, Si-a-C:H and a-C:H:W coatings respectively (Table 6, figure 6 (b)). As a first approximation the compressive plastic strain in these coatings can be assumed to be minimal due to the large radius of the probe used in the test. Haq and co-workers showed that in indentation of DLC films with a 5 μm spherical indenter the localised compressive plastic strain determined by cross-sectional transmission electron microscopic analysis (XTEM) is relatively low (~4%) compared to that induced by Berkovich indentation to the same load [38]. Investigation of the data reported in

XTEM studies by Haq and co-workers clearly shows that the influence of indenter geometry is greater than that of coating thickness [38-41]. In the micro-scratch test the indenter radius was 25 μm so compressive strain in the coating should be minimal. The maximum in von Mises stress appears to coincide with the location of the adhesive layer-gradient layer boundary at the L_{c1} failure on the a-C:H and Si-a-C:H coatings. The maximum in von Mises stress appears to coincide with the location of the substrate-adhesive layer boundary at the L_{c2} failure on the a-C:H and Si-a-C:H coatings.

Although we have made some simplifying assumptions it does appear that for the a-C:H and Si-a-C:H coatings the L_{c1} and L_{c2} events may occur when the maximum stress is closer to interfaces in the multilayer structure. In contrast, for the a-C:H:W coating the L_{c1} and L_{c2} events both occur when the stress maximum is far into the substrate. Schwarzer and co-workers have proposed [31] that (i) plastic flow occurs wherever the critical von Mises stress is exceeded (ii) with increasing load this plastic zone grows until it reaches the interface between the coating and the substrate weakening the integrity of the system (iii) if additionally high tensile stresses at the surface coincide with this weakening then mode-I fractures could propagate to this interface resulting in global coating failure by shearing off large areas (the observed critical load). The failure mechanism on the a-C:H and Si-a-C:H coatings appears to follow a broadly similar progression. Between L_y and L_{c1} the plastic zone grows with cracking occurring when the maximum von Mises, i.e. weakening, stress being centred on the interface between the bonding layer and the graded layer. The cracking at the rear of the moving probe is associated with high tensile stress [42]. It appears that these are cohesive cracks in the sense that they do not propagate to the interface with the substrate and cause debonding. As the load is increased further the maximum stress becomes centred on the interface with the substrate and dramatic debonding occurs. On the a-C:H:W coating the SEM supports a different failure mechanism. Enhanced stress relief due to the greater plastic

deformation results in the maximum stress being driven into the substrate before cracking occurs and the more extreme bending of the coating itself may be responsible for the cracking and film failure.

4.5 Influence of probe geometry and deformation on friction

Although the surface roughness is the same for all three coatings there was a marked difference in friction between them when testing with the sharper probe. The friction force in the nano-scratch test can be deconvoluted into its interfacial and ploughing components so that the interfacial friction can be reported (Eqn. 6):-

$$\mu_{\text{total}} = \mu_{\text{interfacial}} + \mu_{\text{ploughing}} \quad [\text{Eqn. 6}]$$

The friction coefficient at yield is commonly reported to be ~0.05-0.1 for carbon films when sliding against spherical diamond probes [9, 42]. Differences in elastic deformation and plastic ploughing have a marked influence on the evolution of the friction vs. load in the nano-scratch test. Lower deformation on the a-C:H and Si-a-C:H coatings results in a smaller ploughing contribution to the total friction. The ploughing contribution is small at yielding, nevertheless differences remain so it can be inferred that the lower total friction on coating A is due to both lower ploughing and lower interfacial friction.

The use of a larger radius probe enables the ploughing contribution to the total friction to be minimized so that the interfacial friction can be more accurately determined. The slight difference (offset by ~0.03) between friction coefficients at yield determined with the 5 and 25 μm probes may reflect surface roughness, change in the location of yield and/or increased elastic ploughing with the smaller radius probe. As the on-load depth data with the $R = 25 \mu\text{m}$

probe are initially almost identical for the three coatings so the ploughing contributions to the total measured friction are the same. This marked difference to the nano-scratch behaviour where higher hardness reduces deformation and ploughing is due to the larger radius and more substrate-dominated response. With the 25 μm probe the a-C:H and Si-a-C:H coatings show very similar frictional behaviour, with friction coefficients of 0.07 at the onset of yield. The a-C:H:W coating has higher friction of 0.1 at the onset of non-elastic deformation (figure 4 (f)). The variation of friction vs. load follows the same trend for all three, only offset slightly higher for the a-C:H:W coating (figure 4 (e)). Since the ploughing contribution is essentially identical the larger total friction on the a-C:H:W is due to a higher interfacial friction component.

5. Conclusions

There was a marked correlation between the nanomechanical behaviour of the coatings and their tribological response. By employing nano- and micro-scale tribological testing with probes of differing sharpness it has proved possible to alter the sensitivity of the scratch test to probe the response of the coating top layer or the entire multilayer coating-substrate system. Although a clear relationship exists between the ratio of hardness to reduced modulus and the ratio of plastic to total work done in the indentation test (the plasticity index), the apparent constant of proportionality between them varied, being lower for lower plasticity coatings. Plastic deformation is a major source of stress relaxation in the scratch test and the coating with higher plasticity index did not crack before the maximum load in the nano-scratch test was reached. Friction and yield stress were found to strongly depend on the test probe radius. With a suitable choice of test probe geometry ($R = 5 \mu\text{m}$) the Hertzian analysis is able to provide a measure of the coating yield stress that is similar to that previously

estimated by analytical treatment of nanoindentation data. The friction force can be separated into interfacial and ploughing components. The different contributions to the ploughing component of the friction in the nano- and micro-scale scratch tests result in a different dependence of friction vs. load. In the nano-scratch test the coating hardness (and Y/E) affects the extent of deformation and ploughing. The nano-scratch measurements show that a-C:H:W has a higher interfacial and ploughing friction force. In the micro-scratch test with the larger 25 μm probe the stress field extends further towards the substrate resulting in similar deformation (on-load and residual scratch depths) and ploughing contribution to the total friction force. The maximum von Mises stress appears to coincide with the location of the adhesive layer-gradient layer boundary at the L_{c1} failure and with the location of the substrate-adhesive layer boundary at the L_{c2} failure on the a-C:H and Si-a-C:H coatings. The a-C:H:W coating with higher plasticity index exhibited much higher critical loads for fracture (L_{c1}) and total film failure (L_{c2}). SEM supports a different failure mechanism for this coating where enhanced stress relief due to the greater plastic deformation results in the maximum stress being driven into the substrate before cracking occurs.

6. References

1. J. Robertson, Diamond-like amorphous carbon, *Materials Science and Engineering*, R 37 (2002), 129-281.
2. *Tribology of Diamond-like Carbon Films: Fundamentals and Applications*, C. Donnet and A. Erdemir (Eds.), Springer, 2008.
3. T.W. Liskiewicz, B.D. Beake, N. Schwarzer and M.I. Davies, Short note on improved integration of mechanical testing in predictive wear models, *Surf Coat Technol* 237 (2013) 212.

4. N. Schwarzer, Scale invariant mechanical surface optimisation applying analytical time-dependent contact mechanics for layered structures, (2015) pp287-328 in Surface Modification Technologies XXVIII, Eds. TS Sudarshan, P Vuoristo and H. Koivuluoto.
5. A. Gies, T. Chudoba, N. Schwarzer, J. Becker, Influence of the coating structure of a-C:H:W coatings on their wear-performance: A theoretical approach and its practical confirmation, Surface & Coatings Technology 237 (2013) 299-304.
6. J. Jiang and R.D. Arnell, On the running-in behaviour of diamond-like carbon coatings under the ball-on-disk contact geometry, wear 217 (1998) 190-199.
7. R. Gåhlin, M. Larsson, P. Hedenqvist, ME-C:H coatings in motor vehicles, Wear 249 (2001) 302-309.
8. X.T. Zeng, S. Zhang, X.Z. Ding, D.G. Teer, Comparison of three types of carbon composite coatings with exceptional load-bearing capacity and high wear resistance, Thin Solid Films 420-421 (2002) 366-370.
9. Nano-scratch, nanoindentation and fretting tests of 5–80 nm ta-C films on Si(100), BD Beake, MI Davies, TW Liskiewicz, VM Vishnyakov and SR Goodes, Wear, 301 (2013) 575-582.
10. B.D. Beake, T.W. Liskiewicz and J.F. Smith, Deformation of Si(100) in spherical contacts – Comparison of nano-fretting and nano-scratch tests with nano-indentation, Surf. Coat. Technol., 206 (2011) 1921-1926.
11. Review of recent progress in nanoscratch testing, BD Beake, AJ Harris and TW Liskiewicz, Tribology 7 (2013) 87-96.
12. A. Leyland and A. Matthews, On the significance of the H/E ratio in wear control: a nanocomposite coating approach to optimised tribological behaviour Wear 246, (2000) 1-11.

13. A. Leyland and A. Matthews, Design criteria for wear-resistant nanostructured glassy-metal coatings, *Surf. Coat. Technol.*, 177-178 (2004) 317-324.
14. G.S. Fox-Rabinovich, S.C. Veldhuis, V.N. Scvorstov, L.S. Shuster, G.K. Dosbaeva, Elastic and plastic work of indentation as a characteristic of wear behavior for cutting tools with nitride PVD coatings, *Thin Solid Films*, 469-470 (2004) 505.
15. Ben D. Beake and Tomasz W. Liskiewicz, Nanomechanical characterization of carbon films, in press.
16. B.D. Beake, S.R. Goodes and B. Shi, Nanomechanical and nanotribological testing of ultra-thin carbon-based and MoST films for increased MEMS durability, *J. Phys. D: Appl. Phys.* 42 (2009) 065301.
17. Y.-T. Cheng and C.-M. Cheng, Relationships between hardness, elastic modulus, and the work of indentation, *Appl. Phys. Lett.* 73 (1998) 614-616.
18. Y.-T. Cheng and C.-M. Cheng, Scaling, dimensional analysis, and indentation measurements, *Mater. Sci. Eng. R* 44 (2004) 91-149.
19. B.D. Beake, G.S. Fox-Rabinovich, S.C. Veldhuis and S.R. Goodes, Coating optimisation for high-speed machining with advanced nanomechanical test methods *Surf Coat Technol* 203 (2009) 1919-1925.
20. Y. Choi, H.-S. Lee and D. Kwon, Analysis of sharp-tip indentation load-depth curve for contact area determination taking into account pile-up and sink-in effects, *J. Mater. Res.* 19 (2004) 3307-3315.
21. B.D. Beake, S.R. Goodes, J.F. Smith, G.S. Fox-Rabinovich and S.C. Veldhuis, Using nanomechanics to optimise coatings for cutting tools, in *Handbook of Nanostructured Thin Films and Coatings, Mechanical Properties*, Chapter 6, pp205-244, Ed. S Zhang, CRC Press (2010).

22. B.D. Beake, G.S. Fox-Rabinovich, Y. Losset, K. Yamamoto et al, Why can TiAlCrSiYN-based adaptive coatings deliver exceptional performance under extreme frictional conditions? *Faraday Discussions* 156 (2012) 267-278.
23. K.K. Jha, N. Suksawang and A. Agarwal, A new insight into the work-of-indentation approach used in the evaluation of material's hardness from nanoindentation measurement with Berkovich indenter, *Computational Materials Science* 85 (2014) 32–37.
24. D Tabor, *The Hardness of Metals*, Clarendon Press, Oxford, UK, 1951, ISBN: 0-521-29183-6.
25. B. Shi, J.L. Sullivan and B.D. Beake, An investigation into which factors control the nanotribological behaviour of thin sputtered carbon films, *J Phys D:Appl Phys* 41 (2008) 045303.
26. S. Zhang, X.L. Bui, Y. Fu and H. Du, Development of carbon-based coating on extremely high toughness with good hardness, *Int. J. Nanosci.* 3 (2004) 571-578.
27. S. Zhang, X.L. Bui, Y. Fu, D.L. Butler and H. Du, Bias-graded deposition of diamond-like carbon for tribological applications, *Diam. Relat. Mater.* 13 (2004) 867-871.
28. Y.X. Wang and S. Zhang, Toward hard yet tough ceramic coatings, *Surf. Coat. Technol.* 258 (2014) 1-16.
29. A.C. Fischer-Cripps, Critical review of analysis and interpretation of nanoindentation test data, *Surf. Coat. Technol.* 200 (2006) 4153-4165.
30. K.L. Johnson, *Contact Mechanics*, Cambridge University Press, London, UK, 1985, ISBN: 0-521-34796-3.
31. N. Schwarzer, Q.-H. Duong, N. Bierwisch, G. Favaro, M. Fuchs, P. Kempe, B. Widrig and J. Ramm, *Surf. Coat. Technol.*, 206 (2011) 1327-1335.

32. S. Zhang, D. Sun, Y. Fu and H. Du, Effect of sputtering target power on microstructure and mechanical properties of nanocomposite nc-TiN/a-SiN_x thin films, *Thin Solid Films*, 447–8 (2004) 462-467.
33. S. Zhang, D. Sun, Y. Fu and H. Du, Toughness measurement of thin films: a critical review, *Surf. Coat. Technol.*, 198 (2005) 74-84.
34. B.D. Beake, V.M. Vishnyakov, R. Valizadeh, J.S. Colligon, Influence of mechanical properties on the nanoscratch behaviour of hard nanocomposite TiN/Si₃N₄ coatings on Si, *J Phys D: Appl Phys* 39 (2006) 1392-1397.
35. G.S. Fox-Rabinovich, B.D. Beake, S.C. Veldhuis, J.L. Endrino, R. Parkinson, L.S. Shuster, M.S. Migranov, Impact of mechanical properties measured at room and elevated temperatures on wear resistance of cutting tools with TiAlN and AlCrN coatings, *Surf Coat Technol* 200 (2006) 5738-5742.
36. G.S. Fox-Rabinovich, J.L. Endrino, B.D. Beake, A.I. Kovalev, S.C. Veldhuis, L. Ning, F. Fotaine and A. Gray, Impact of annealing on the microstructure, properties, and cutting performance of AlTiN coating, *Surf Coat Technol* 201 (2006) 3524-3529.
37. G.S. Fox-Rabinovich, B.D. Beake, K. Yamamoto, M.H. Aguirre, S.C. Veldhuis, G. Dosbaeva, A. Elfizy, A. Biksa, and L.S. Shuster, A.Y. Rashkovskiy, Structure, properties and wear performance of nano-multilayered TiAlCrSiYN/TiAlCrN coatings during machining of Ni-based aerospace superalloys, *Surf. Coat. Technol.* 204 (2010) 3698-3706.
38. A.J. Haq, P.R. Munroe, M. Hoffman, P.J. Martin, A. Bendavid, Berkovich indentation of diamond like carbon coatings on silicon substrates, *J. Mater. Res.* 23 (2008) 1862-1869.

39. A.J. Haq, P.R.Munroe, M.Hoffman, P.J.Martin and A.Bendavid, Nanoindentation-induced deformation behaviour of tetrahedral amorphous carbon coating deposited by filtered cathodic vacuum arc, *Diamond and Related Materials* 19 (2010) 1423-1430.
40. A.J. Haq, P.R.Munroe, M.Hoffman, P.J.Martin and A.Bendavid, Nanoindentation-induced deformation behaviour of diamond-like carbon coatings on silicon substrates, *Thin Solid Films* 515 (2006) 1000-1004.
41. A.J. Haq, P.R.Munroe, M.Hoffman, P.J.Martin and A.Bendavid, Effect of coating thickness on the deformation behaviour of diamond-like carbon-silicon system, *Thin Solid Films* 518 (2010) 2021–2028.
42. K. Holmberg, H. Ronkainen, A. Laukkanen, K. Wallin, A. Erdemir and O. Eryilmaz, Tribological analysis of TiN and DLC coated contacts by 3D FEM modelling and stress simulation, *Wear*, 264 (2008) 877-884.

Tables

Table 1 Multilayer coating architecture

Short name	Layer structure	Adhesive layer (μm)	Gradient layer (μm)	DLC layer (μm)	Total (μm)
a-C:H	Cr+W-C:H+DLC	0.3 (Cr)	0.7 (W-C:H)	2.9 (DLC)	3.9
Si-a-C:H	Cr+W-C:H+Si-DLC	0.3 (Cr)	0.7 (W-C:H)	2.8 (Si-DLC)	3.8
a-C:H:W	CrN+a-C:H:W	1.0 (CrN)	-	2.0 (a-C:H:W)	3.0

Table 2 Nanoindentation results at 40 mN

	H (GPa)	E_r (GPa)	h_c (nm)	H/E_r	H^3/E_r^2 (GPa)
a-C:H	25.0 ± 1.1	194.7 ± 5.4	227.1 ± 5.9	0.128 ± 0.003	0.41 ± 0.04
Si-a-C:H	16.3 ± 0.5	143.3 ± 2.9	287.3 ± 4.7	0.114 ± 0.002	0.21 ± 0.01
a-C:H:W	12.7 ± 1.7	157.1 ± 13.3	331.9 ± 26.5	0.081 ± 0.005	0.08 ± 0.02

Table 3 Critical load for non-elastic deformation in the nano-scratch test with $R = 5 \mu\text{m}$ probe

	L_y (nano-scratch) (mN)	On-load depth at yield (nm)	Friction coefficient at yield
a-C:H	206 ± 5	604 ± 18	0.115 ± 0.002
Si-a-C:H	110 ± 10	425 ± 26	0.117 ± 0.007
a-C:H:W	68 ± 4	332 ± 21	0.145 ± 0.005

Table 4 Probe depths at critical loads in the micro-scratch test with $R = 25 \mu\text{m}$ probe

Coating	On-load depth (nm)	Residual depth (nm)	% Scratch recovery
a-C:H at L_{c1}	1720 ± 87	652 ± 48	62.1 ± 2.5
a-C:H at L_{c2}	2028 ± 112	718 ± 82	64.6 ± 5.5
Si-a-C:H at L_{c1}	1475 ± 102	586 ± 61	60.2 ± 3.4
Si-a-C:H at L_{c2}	1794 ± 96	693 ± 63	61.3 ± 4.3
a-C:H:W at L_{c1}	2137 ± 251	1021 ± 167	52.2 ± 2.9
a-C:H:W at L_{c2}	2747 ± 105	1357 ± 67	50.6 ± 1.0

Table 5 Yield pressures from nano-scratch and nanoindentation tests

	Y (nano-scratch) (GPa)	Y (nanoindentation analysis) (GPa)
a-C:H	20.6 ± 0.9	23.8
Si-a-C:H	14.9 ± 0.5	14.3
a-C:H:W	12.4 ± 0.8	12.0

Table 6 Hertzian analysis of micro-scratch test results with $R = 25 \mu\text{m}$ probe

Coating	Contact depth (nm)	Maximum von Mises stress (GPa)	Depth of maximum von Mises stress (nm)
a-C:H at L_{c1}	1186 ± 60	12.0 ± 0.3	3633 ± 69
a-C:H at L_{c2}	1373 ± 49	12.4 ± 0.4	3921 ± 68
Si-a-C:H at L_{c1}	1031 ± 73	12.6 ± 0.3	3408 ± 118
Si-a-C:H at L_{c2}	1244 ± 53	11.8 ± 0.3	3737 ± 79
a-C:H:W at L_{c1}	1583 ± 201	11.7 ± 0.4	4195 ± 261
a-C:H:W at L_{c2}	2052 ± 85	11.9 ± 0.1	4760 ± 95

Figure captions

1. (a-c) Depth-dependence of the relationship between plasticity index (PI), H/E_r and the apparent constant of proportionality when using a Berkovich indenter (a) on a-C:H; (b) on Si-a-C:H and (c) on a-C:H:W. (d) The relationship between PI and H/E_r for the coatings at a contact depth of 300 nm.
2. Load-dependence of friction coefficient in nano-scratch test using $R = 5 \mu\text{m}$ probe
3. SEM images of nano-scratch tracks with $R = 5 \mu\text{m}$ probe. The scratch direction is from top right to bottom left. (a) a-C:H. x12000 magnification image of the end of the nano-scratch track (500 mN). (b) Si-a-C:H. x16000 magnification image near of the nano-scratch track (>450 mN). (c) a-C:H:W. x10000 magnification image midway through the nano-scratch track (>250 mN).
4. Micro-scratch test using $R = 25 \mu\text{m}$ probe. (a) Critical loads (b) On-load probe depth (c) residual depth (d) Load-dependence of elastic recovery in micro-scratch testing with $R = 25 \mu\text{m}$ probe. (e) Variation in friction coefficient with applied load (f) Friction coefficient at L_y , L_{c1} and L_{c2} .
5. SEM images of micro-scratch tracks with $R = 25 \mu\text{m}$ probe. The scratch direction is from top right to bottom left. (a) a-C:H - x6000 magnification image showing cracking above L_{c1} (b) a-C:H - x217 magnification image (c) Si-a-C:H – x227 magnification image (d) a-C:H:W x4000 magnification image showing cracking (e) a-C:H:W – x227 magnification image.
6. Hertzian analysis of micro-scratch test data (a) Mean pressure vs. applied load (b) Location of the maximum von Mises stress below the free surface.

Figures

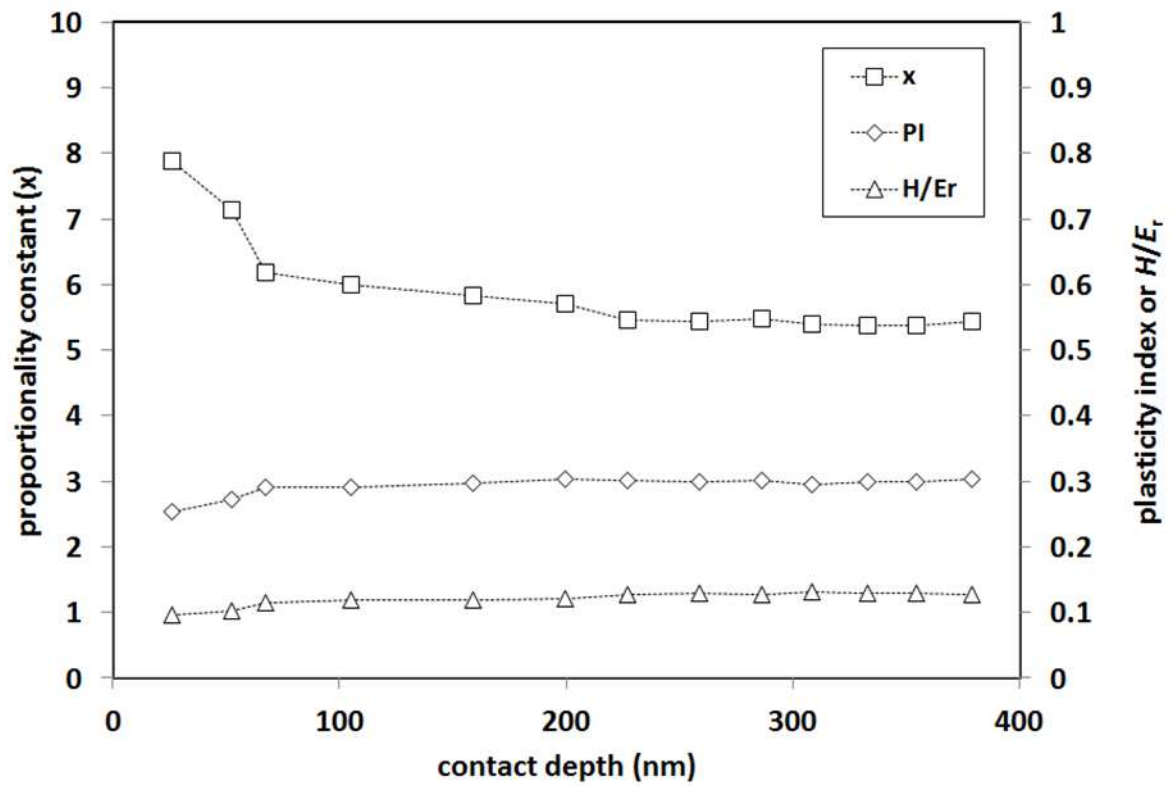


Figure 1. (a)

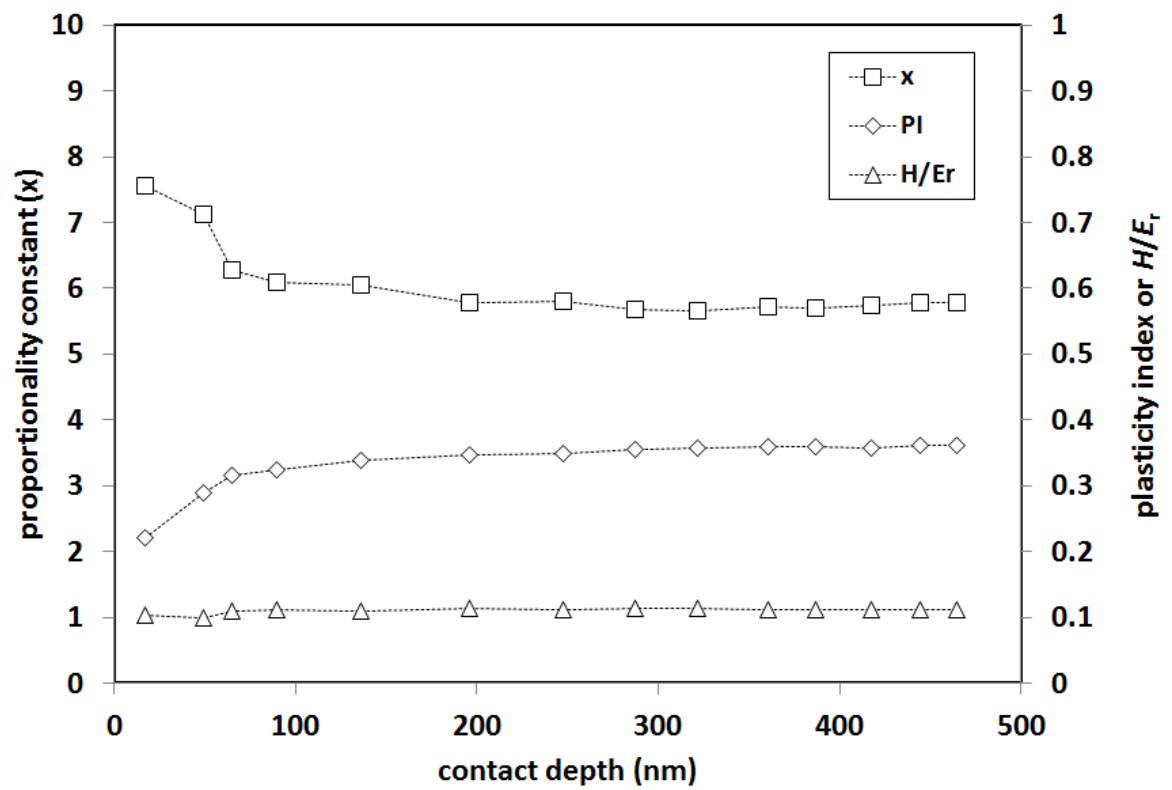


Figure 1. (b)

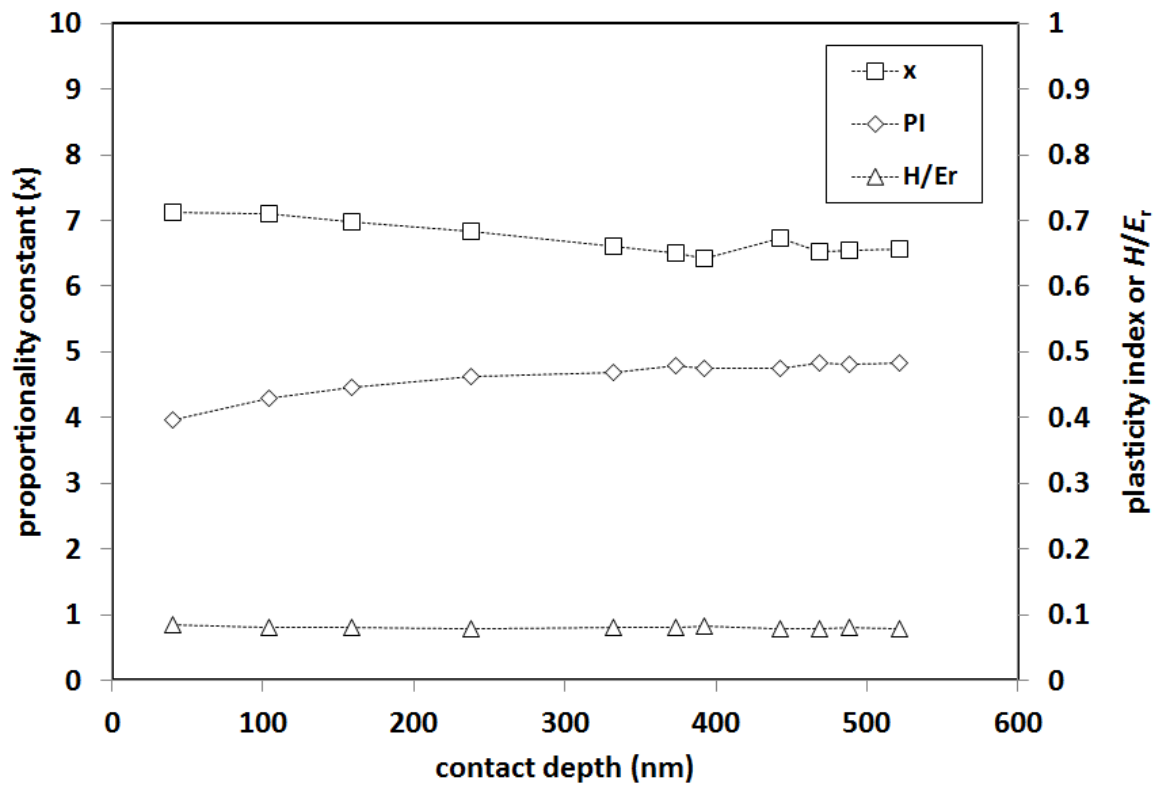


Figure 1. (c)

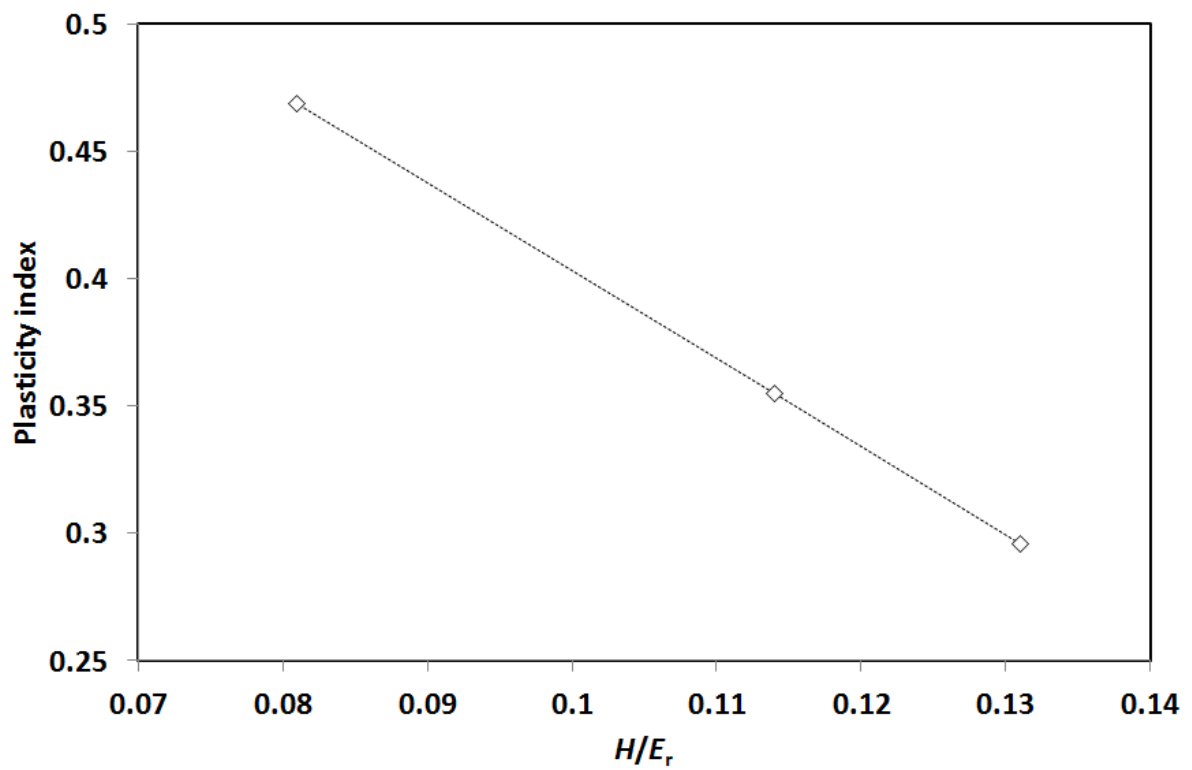


Figure 1. (d)

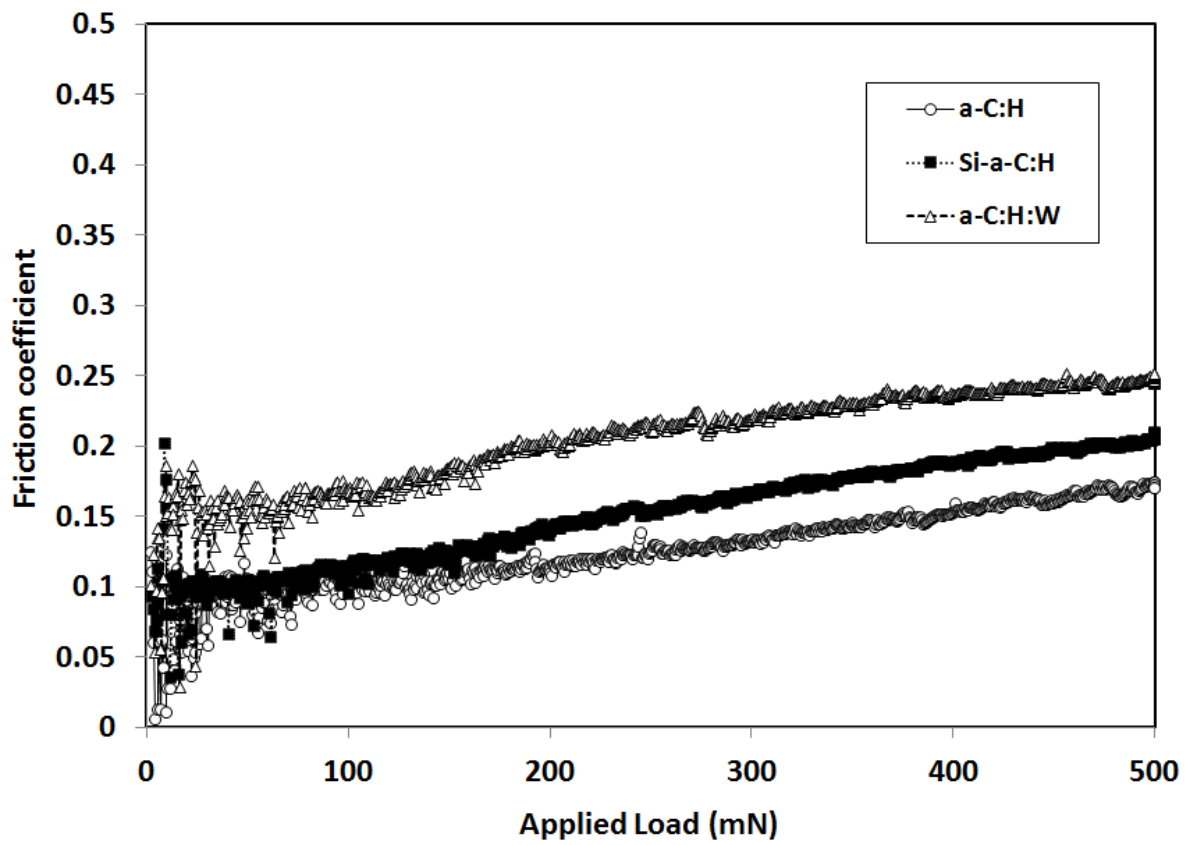


Figure 2.

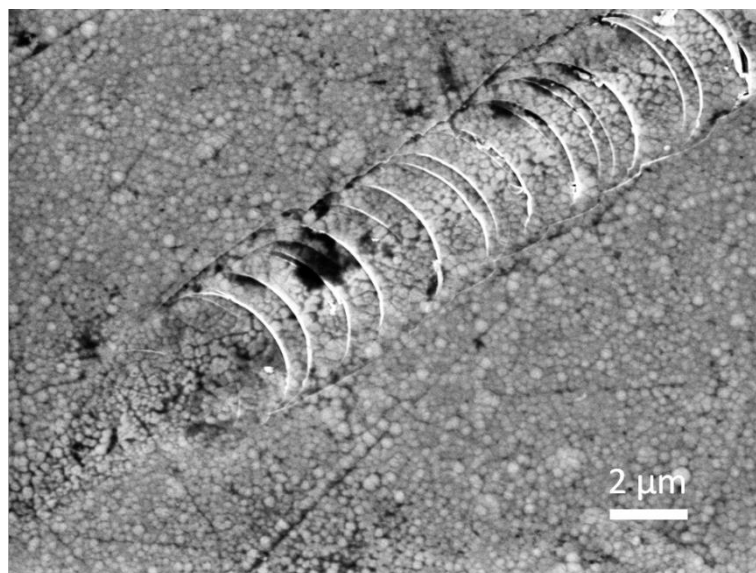


Figure 3. (a)

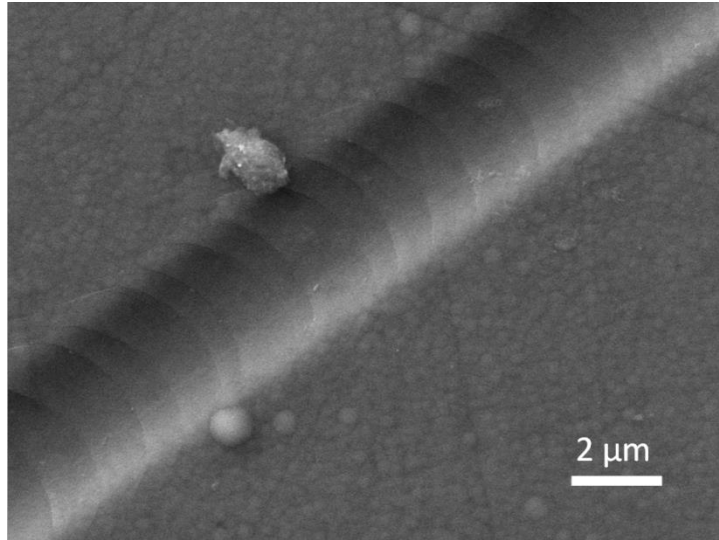


Figure 3(b)

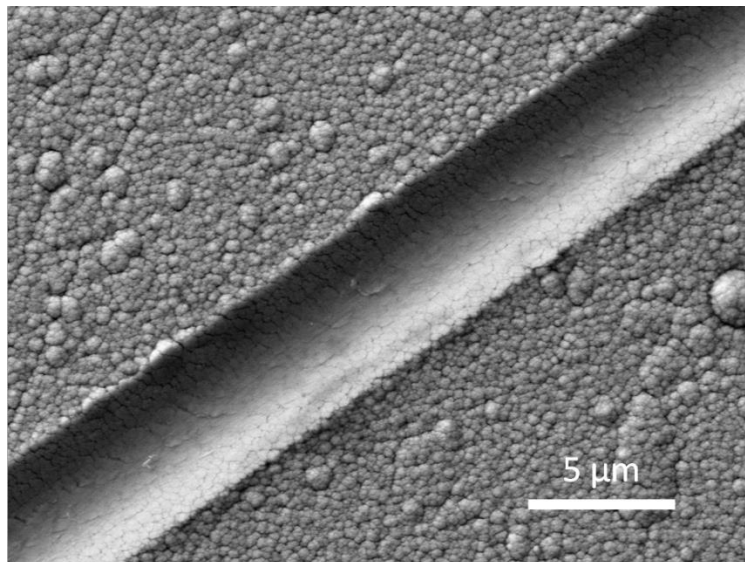


Figure 3 (c)

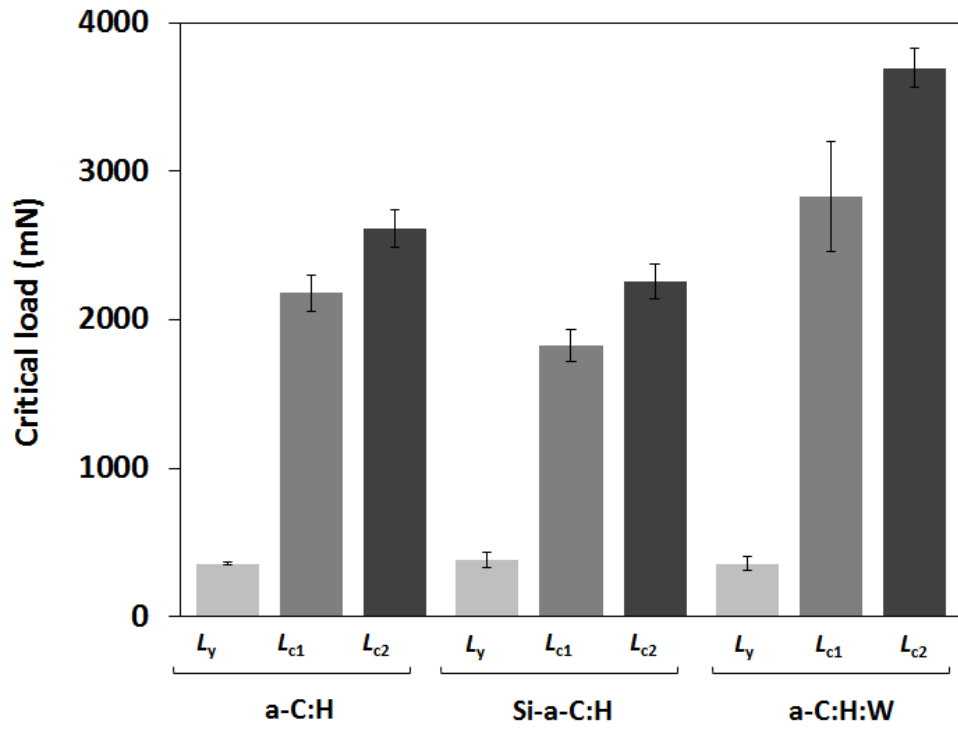


Figure 4 (a)

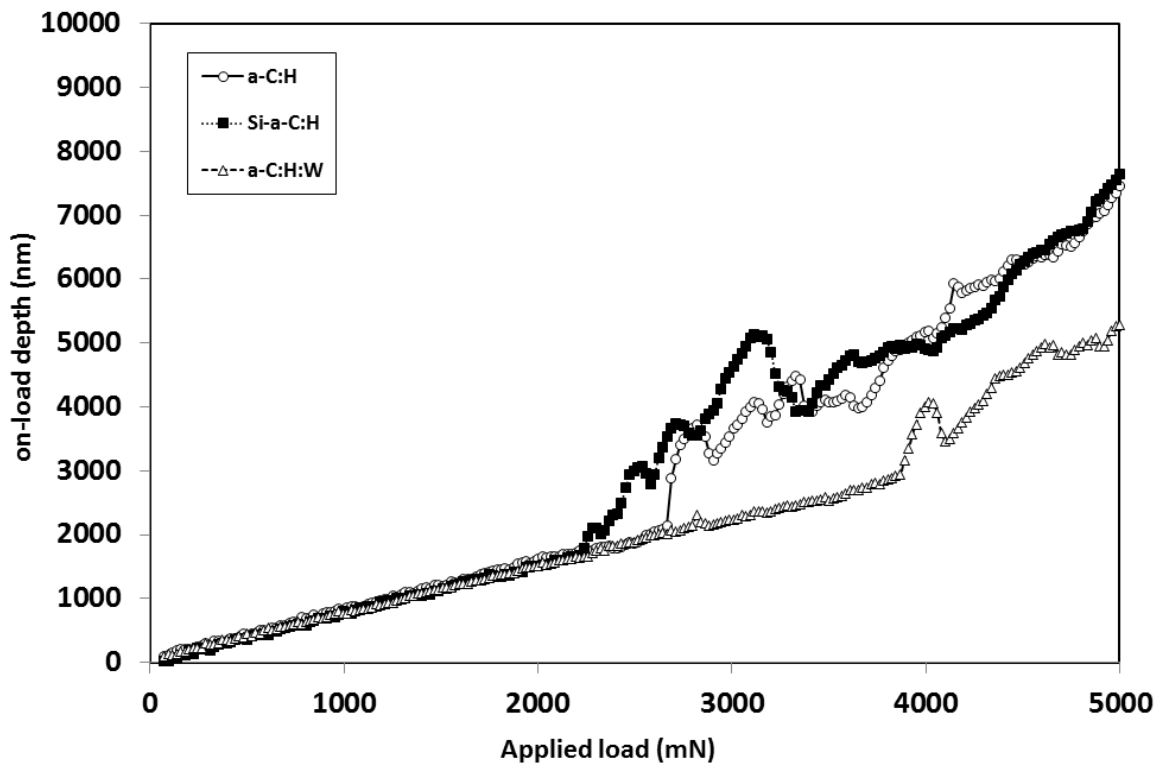


Figure 4 (b)

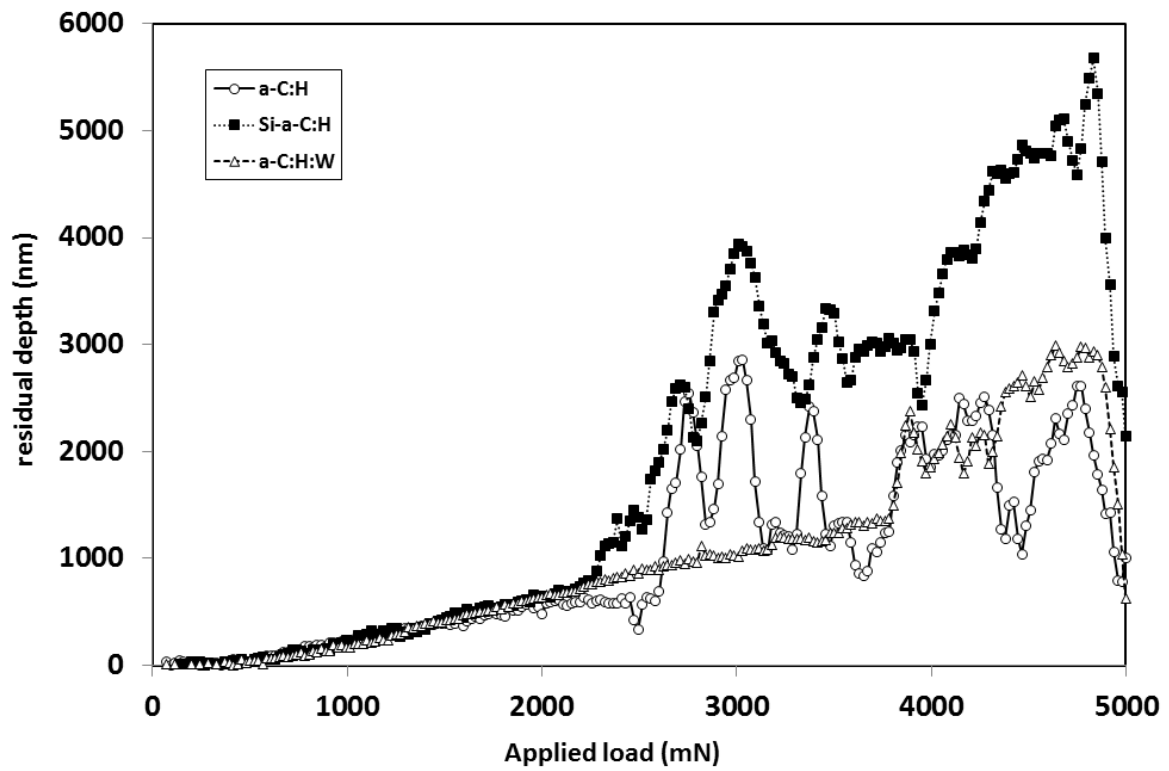


Figure 4 (c)

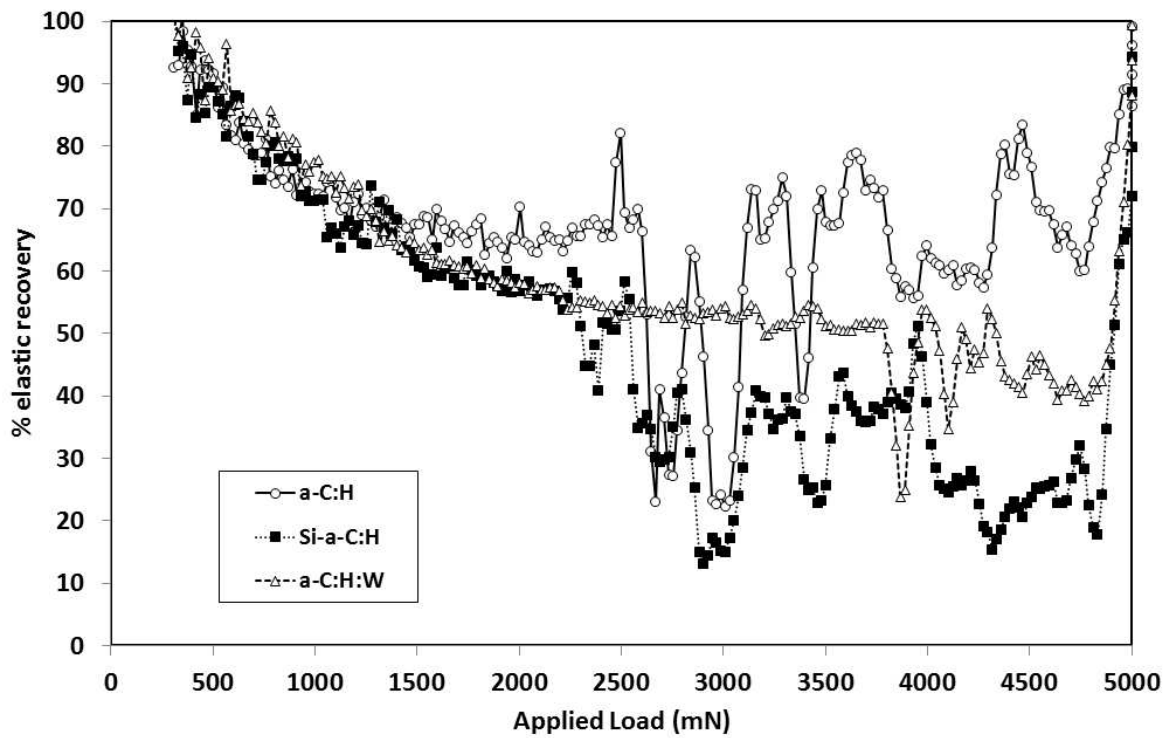


Figure 4 (d)

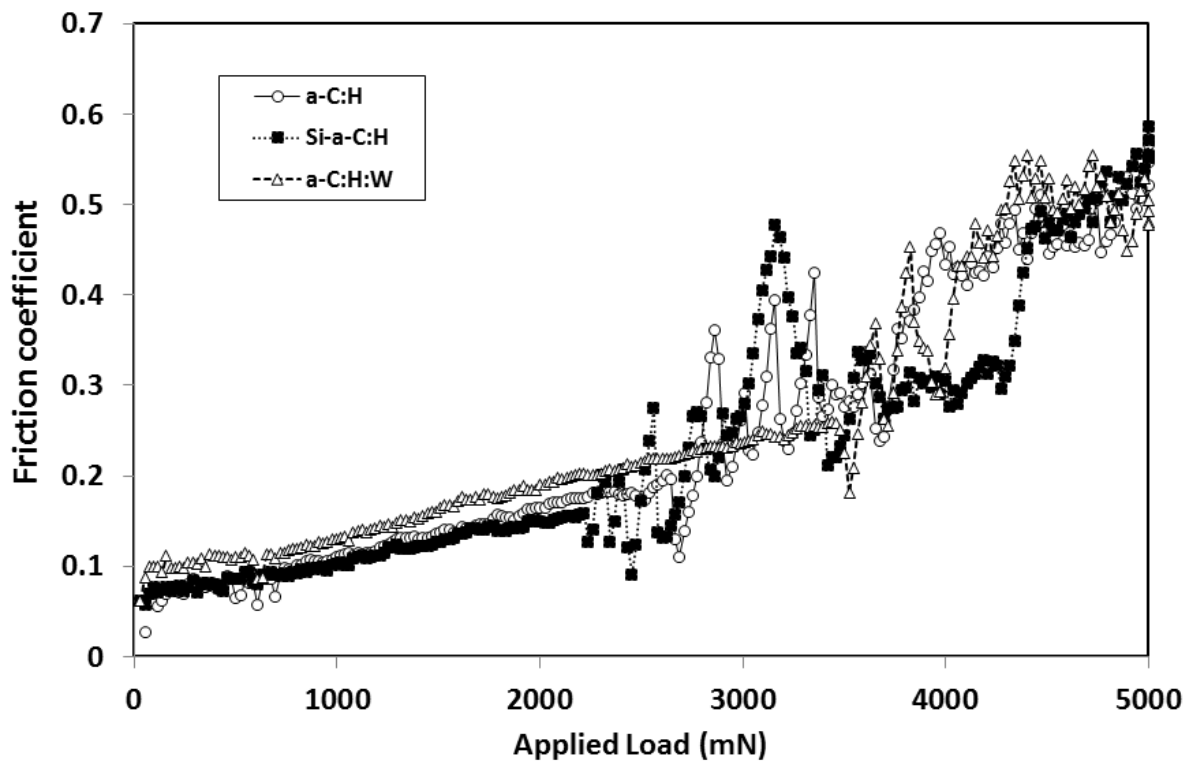


Figure 4 (e)

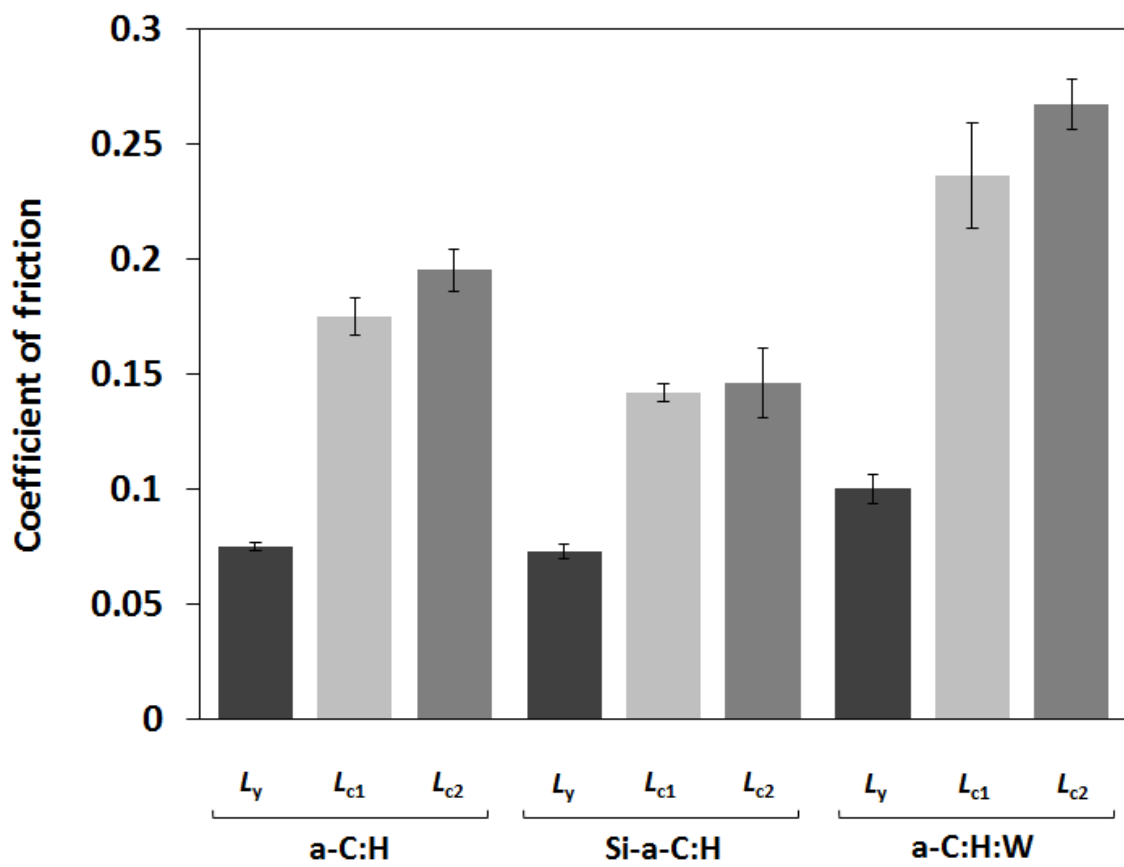


Figure 4 (f)

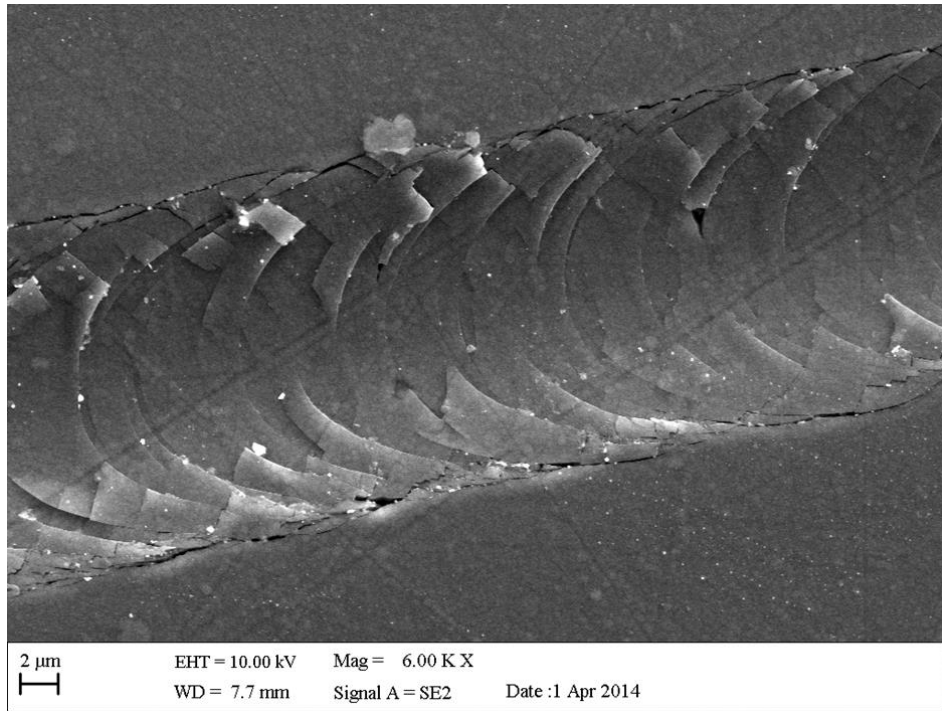


Figure 5. (a)

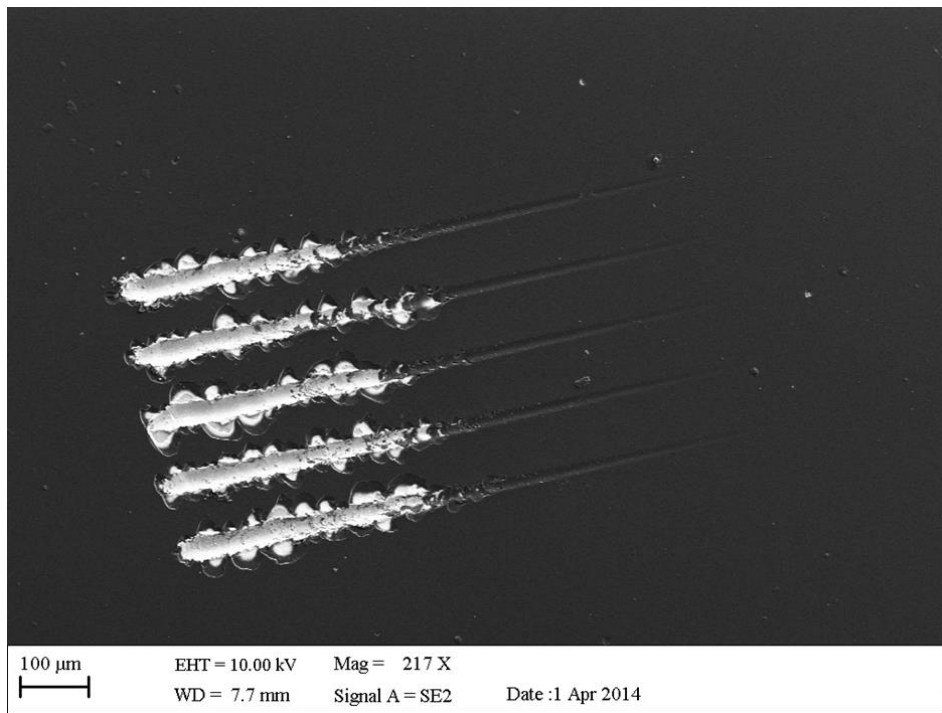


Figure 5. (b)

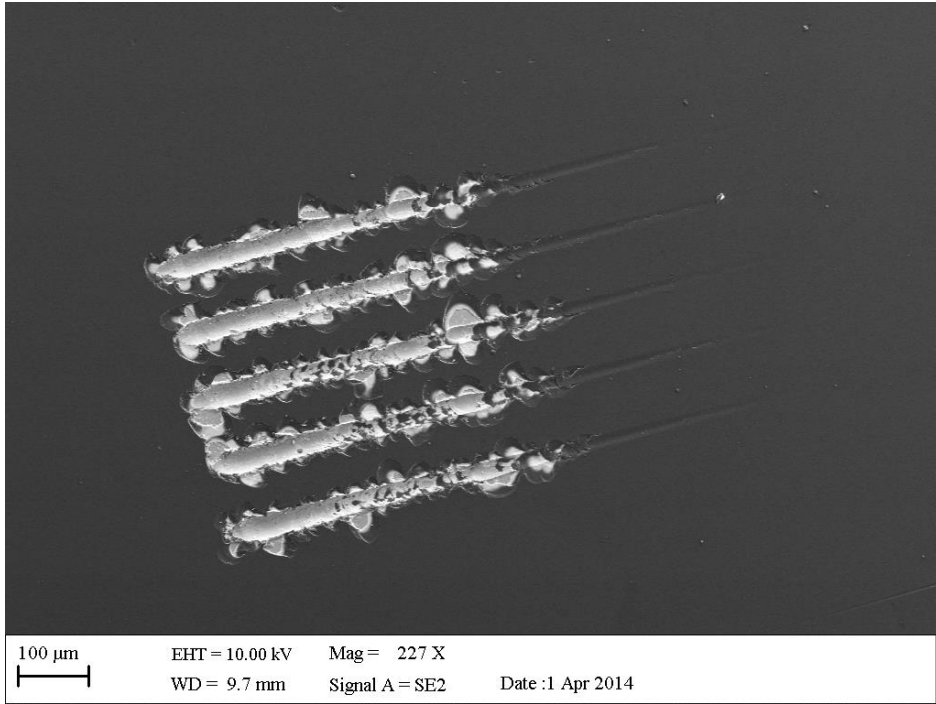


Figure 5 (c).

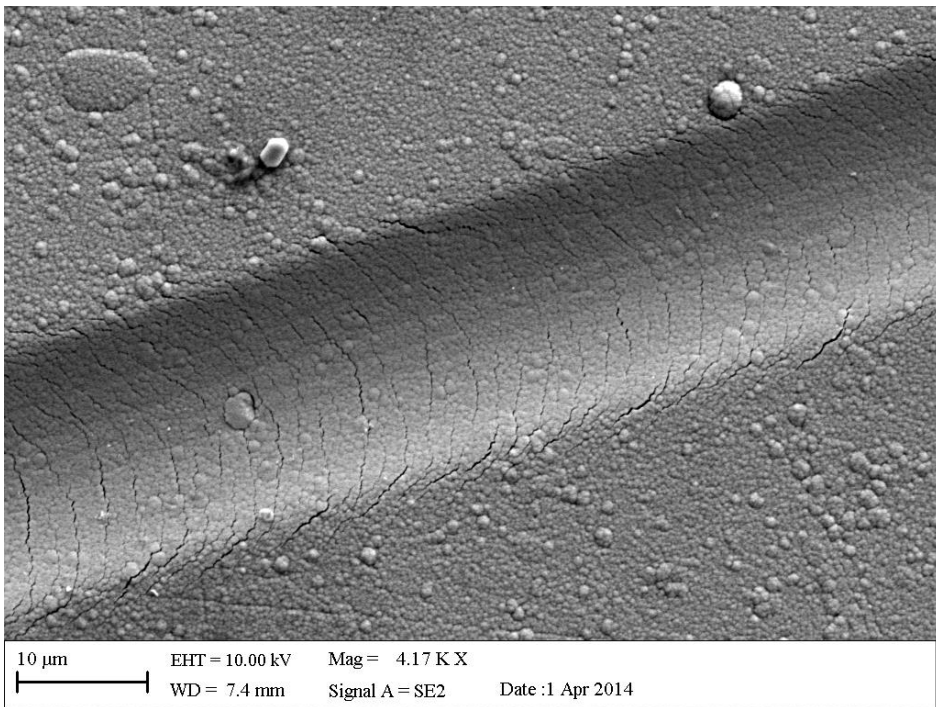


Figure 5 (d)

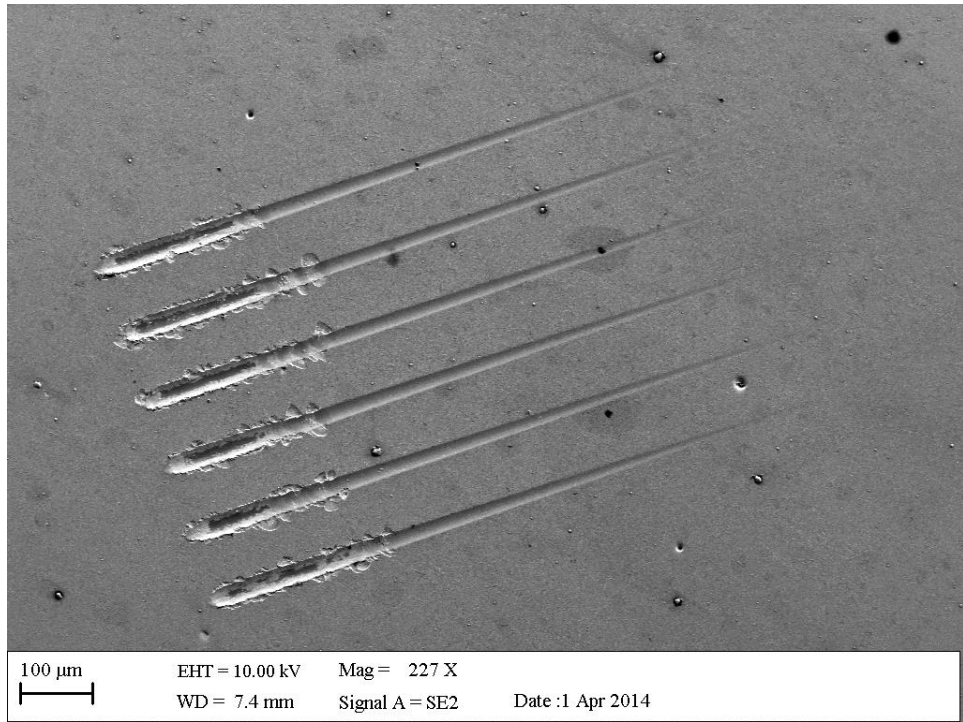


Figure 5 (e)

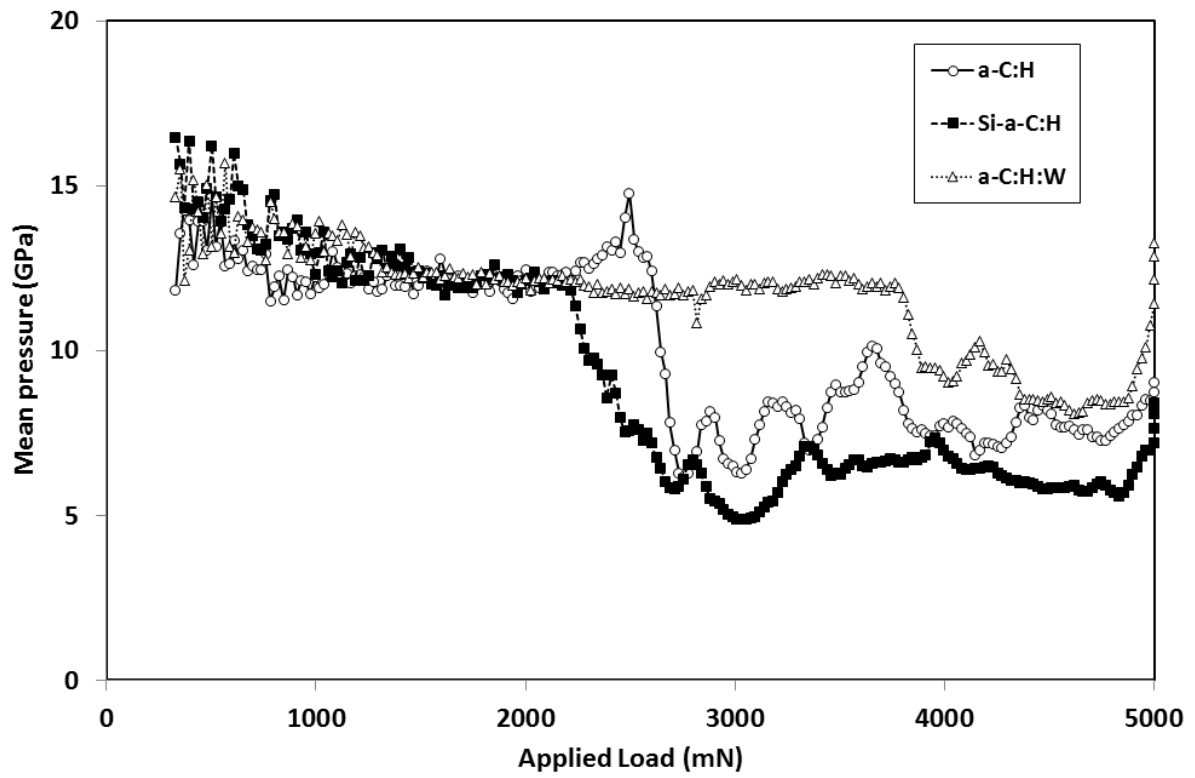


Figure 6 (a)

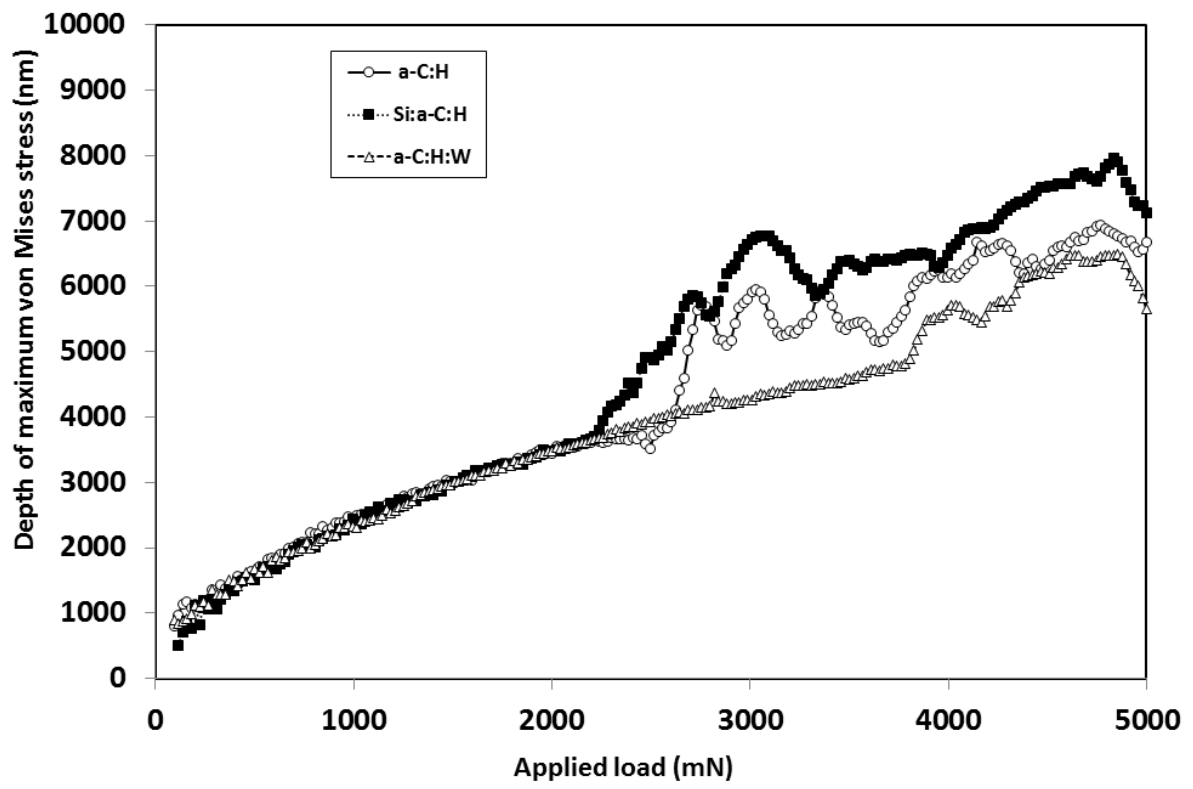


Figure 6 (b)